# Broadband Low-Frequency Acoustic Metamuffler

Lang Shen, Yifan Zhu, Feilong Mao, Siyuan Gao, Zihao Su, Zhitao Luo, Hui Zhang, Badreddine Assouar

# Broadband Low-Frequency Acoustic Metamuffler

Lang Shen[1†], Yifan Zhu[2†], Feilong Mao[1], Siyuan Gao[1], Zihao Su[1], Zhitao Luo[1], Hui Zhang[1*], Badreddine Assouar[2*]

[1]*Jiangsu Key Laboratory for Design and Manufacture of Micro-Nano Biomedical Instruments, School of Mechanical Engineering, Southeast University, Nanjing 211189, China*

[2] *Université de Lorraine, CNRS, Institut Jean Lamour, 54000 Nancy, France.*

**Abstract**

In this research, we propose and design an acoustic metamuffler (AMM) by coupling a micro-perforated plate and a composite waveguide formed by a main waveguide and a Helmholtz resonator. The proposed mechanism and the deliberately designed structure are conducive to generating multimode resonances which help to improve the coupling absorption effect and lead to a broadband (4 octaves) sound insulation. We develop an effective circuit model to analytically predict the insulation bandwidth and put forward numerical and experimental measurements that demonstrate the effectiveness of the proposed concept. The designed AMM produces sound insulation with an average of 20 dB of sound transmission loss at a low frequency range extending from 100 to 1600 Hz while having an ultrathin thickness of 6.2 cm (1/55$\lambda$ for the lowest working frequency). Our findings could have pragmatic applications for acoustic insulators or absorbers.

**Keywords**: acoustic metasurfaces and metamaterials; acoustic insulation; noise control

These authors contributed equally: Lang Shen, Yifan Zhu

**Corresponding authors:**

* seuzhanghui@seu.edu.cn

* badreddine.assouar@univ-lorraine.fr

## I. Introduction

In acoustic engineering, it is a key scientific problem to understand how to achieve low frequency and broadband noise cancellation with small thickness, while maintaining air circulation or ventilation. Traditional sound-absorbing materials and sound barriers not only need huge structural sizes (windows, walls, etc.) to eliminate low frequency noise, but also cannot guarantee air circulation while eliminating noise [1]. Acoustic metamaterials [2-3] and acoustic metasurfaces [4] can achieve the regulations of low-frequency acoustic waves with subwavelength structural sizes, such as negative refraction, acoustic stealth, acoustic abnormal reflections, etc. [5-7]. Thanks to the great success of acoustic metamaterials and acoustic metasurfaces for low-frequency acoustic wave manipulations, various meta-structures have been applied to the design of sound absorbers for the application of the noise control field [8-10]. By employing local resonance and Fano resonance [11-13], sound waves within a certain frequency range can be dissipated and absorbed in the structures, and such designs make it possible for the subwavelength meta-structure to regulate low-frequency sound waves, which provides a different strategy for low frequency acoustic wave manipulations.

Considering that noise is usually broadband, the realization of low frequency broadband noise cancellation has always been the focus and difficulty of research. The emergence of the coupling structure of multiple resonant modes with optimized structural resonance and acoustic interference provides a different design methodology for broadband sound cancellation [14-17]. Even so, achieving low frequency and broadband sound cancellation under airflow conditions [11-13, 17-20] remains a challenge.

In this paper, we propose and demonstrate an acoustic metasurface muffler (AMM) to achieve low-frequency wideband noise elimination. In a prior study [21], it was illustrated that the tunable acoustic filters can be realized by a composite waveguide consisting of a Helmholtz resonator and the main waveguide. Here, we combine the composite waveguide [21] with micro-perforated plate [22-24] as the building block of the AMM to improve the bandwidth of sound insulation. The designed coupled structure helps to increase the resonant mode density of the system [25], especially at very low frequencies. Based on the principle of acoustic absorption interaction and multi-parameter resonance units, a low-frequency broadband noise elimination is achieved. We first analyze the coupled structure theoretically by developing effective circuit models (acoustic-electric analogy [26]). Then, the effectiveness of the proposed theory is verified through simulation and experiment. Through theory, simulation and

experiment, it is proved that this structure can achieve broadband noise cancellation within the range of 100-1600 Hz (the average noise cancellation amount is higher than 20 dB), and its thickness is only 6.2 cm. The proposed mechanism based on the coupled structure can lead to an ultra-broadband (4 octaves) sound insulation, that outperforms previous broadband designs [14-17]. In addition, putting a micro-perforated panel in a series connections introduces an additional trade-off between ventilation performance and sound insulation, since the micro-perforated plate may block part of the fluid under flowing-fluid-filled circumstances [17]. We therefore have evaluated and optimized the ventilation performance in our case. The most critical factor affecting the ventilation performance of AMM is the ventilation area. Through calculation, it can be concluded that the minimum ventilation area of the AMM designed in this work is about of 81 $mm^2$, accounting for about 13% of the cross-section area.

## II. RESULTS

### A. The coupled silencing structure

As shown in Fig. 1 (a), we draw a conceptual diagram of AMM, that consists of a coupled structure connected by a micro-perforated plate layer and a composite waveguide layer. The structure is a square with a side length $a$=70 mm and total thickness $\boldsymbol{H = h_1 + h_2 + h_3}$. Here $\boldsymbol{h_1 = 2}$ mm is the thickness of the micro-perforated plate. $\boldsymbol{h_2 = 20}$ mm is the thickness of the mid-air layer. $\boldsymbol{h_3 = 40}$ mm is the thickness of the composite waveguide layer. The pore diameter of the top micro-perforated plate is $r$=0.3 mm, and the perforation rate is $\boldsymbol{\sigma = \pi r^2/p^2}$ = 0.4%. The outer parameters of the four units (four units) at the bottom are the same. For clarity, the composite waveguide layer is detached to show the details of its inner structure. It has four kinds of composite waveguide units with different parameters. In each unit, the cross-sectional area of the acoustic main waveguide and the length of the neck is $S_1$ = 4×30 $mm^2$ and $l$=4 mm respectively. The other parameters for four units are shown in Table 1 ($S_2$ is the cross-sectional area of the necks, V is the volume of the Helmholtz cavity).

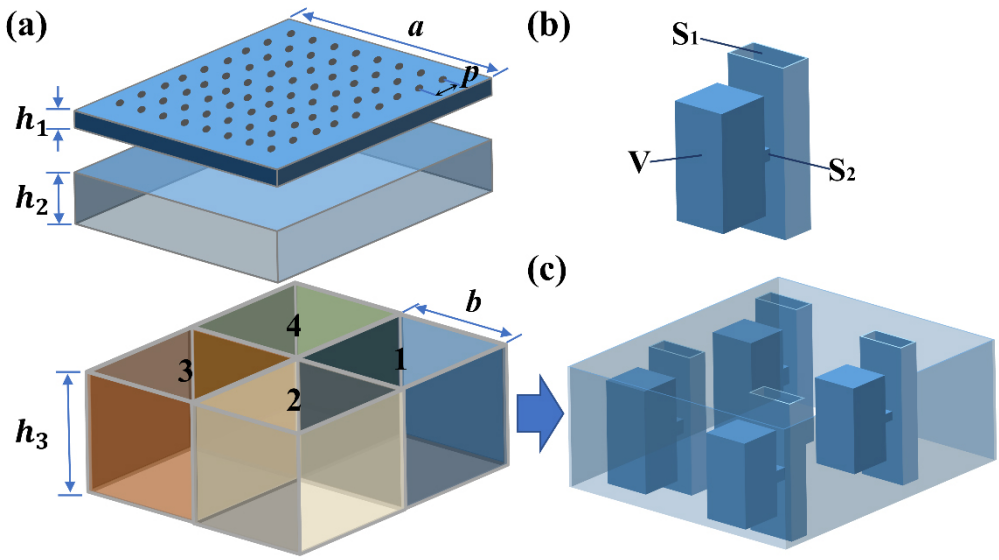


FIG. 1. (a) Schematic diagram of AMM and the unit composition. (b) The composite waveguide units have a different internal size and are divided into three parts: the waveguide, the neck, and the Helmholtz cavity. (c) The composite waveguide layer is composed of four units.

Table 1. Structural parameters of the composite waveguide

| | Unit 1 | Unit 2 | Unit 3 | Unit 4 |
|---|---|---|---|---|
| $S_2$ (mm2) | 1×1 | 2×2 | 3×5 | 5×7.5 |
| V (mm3) | 18000 | 18000 | 22500 | 22500 |

To make the AMM have a broadband muffling effect, each unit has a different sound absorption and isolation frequency band. In addition, on the surface of the structure, we also designed a micro-perforated plate structure whose anechoic frequency band is just complementary to the composite waveguide layer. As it will be shown in Fig. 1(b), four composite waveguides are conceived explicitly so that each one has its contribution (high-efficient dissipation or resonance), and they collectively provide a remarkable sound blocking over a wide frequency range, while the whole structure features a subwavelength thickness.

### B. Theoretical model

The coupled silencing structure is shown in Fig. 1(a). Based on the theoretical analysis, the impedance of the micro-perforated plate is calculated according to the acoustic-electrical analogy method, and then the acoustic transmission characteristics of the resonant structure are calculated by using the local analysis method, to obtain the sound transmission loss (STL) of the whole structure. The STL of the coupling structure is determined by the following formula:

$$STL = 10\log_{10}\frac{1}{t_I} \tag{1}$$

$$t_I = \frac{4}{4cos^2(k_2D) + \left(\frac{Z^2 + Z_0^2}{ZZ_0}\right)^2 sin^2(k_2D)} \tag{2}$$

where $t_I$ is the transmission coefficient of sound intensity, $k_2 = 2\pi f/c_0$ is wave number, $D$ is the width of the structure, $f$ is the frequency of the incident sound wave, $Z = \rho_0 c_0$ is the characteristic impedance of air, $Z_0$ is structural impedance, where $\rho_0$=1.21 kg/m$^3$, $c_0$=343 m/s represent air density and sound velocity in air, respectively.

By using the acoustic-electric analogy, we can calculate the relationship between the acoustic impedance of the structure and the parameters of each structure. It can be seen from Fig. 2(a) that the whole structure satisfies the conditions.

$$P_0 = P_1 + P_2 \tag{3}$$

The complex impedance of each part is assumed to be $Z_1$ and $Z_2$.

$$Z_0 = Z_1 + Z_2 (4)$$

We can figure out the magnitude of $Z_1$ and $Z_2$.

$$Z_1 = R_1 + j\mathrm{X}_{L1} - jX_{C1} \tag{5}$$

$$Z_2 = R_2 + jX_{L2} + \frac{R_2R_3 - X_{L2}X_{L3} + X_{L2}X_{C3} + j(R_3X_{L2} + R_2X_{L3} - R_2X_{C3})}{R_2 + R_3 + j(X_{L2} + X_{L3} - X_{C3})} \tag{6}$$

where the waveguide and micro-perforation plate can be regarded as an inductor $L$ in series with a resistor $R$ at low frequencies, Meanwhile, the Helmholtz resonator (HR) cavity and the cavity-backed are equivalent to a capacitor $C$. $X_L = 2\pi fL$ and $X_C = \frac{1}{2\pi fC}$ express inductive and capacitive reactance. $j$ represents the imaginary unit. Analogous to acoustics and electricity: $L = \rho l/S_2$, $C = \frac{V_0}{\rho_0 c_0^2}$, $V_0$ is the volume of the Helmholtz cavity.

For the micro-perforated plate structure, we can simply calculate its acoustic transmission loss curve. When the aperture of the micro-perforated plate is small, its impedance $Z_1$ can be

expressed as [22]:

$$Z_1 \approx \frac{4}{3} j\omega\rho t + \frac{32\rho\mu t}{d^2} \tag{7}$$

The acoustic transmission loss of the micro-perforated plate structure can be calculated by the following formula.

$$STL = -20\lg\left(1 + \frac{Z_1\sigma}{2\rho c}\right) \tag{8}$$

The green circles line in Fig. 2(b) can be obtained by numerical calculation. The results show that the designed micro-perforated plate structure has good noise reduction performance, and the sound reduction effect is significantly improved within the wider frequency range from 0 to 2000 Hz, theoretically.

For the composite waveguide structure, the calculation formula of the acoustic transmission loss can be obtained as follows**.**

$$t_I = \frac{1}{1 + \frac{\rho^2 c^2}{4S_2^2 X_b^2}} \tag{9}$$

where $X_b = \omega\rho l/S_2 - \rho c^2/\omega V$. The STL of the composite waveguide structure can be obtained by combining Eq. (9) with Eq. (2). Based on Eq. (1) to Eq. (9), we find that the sound transmission loss of AMM highly depends on the parameters of both the micro-perforated panel and the waveguide. Thus, the reasonable design structure parameter can lead to a planar and optimized sound insulation spectrum, considering the coupling effect between structures.

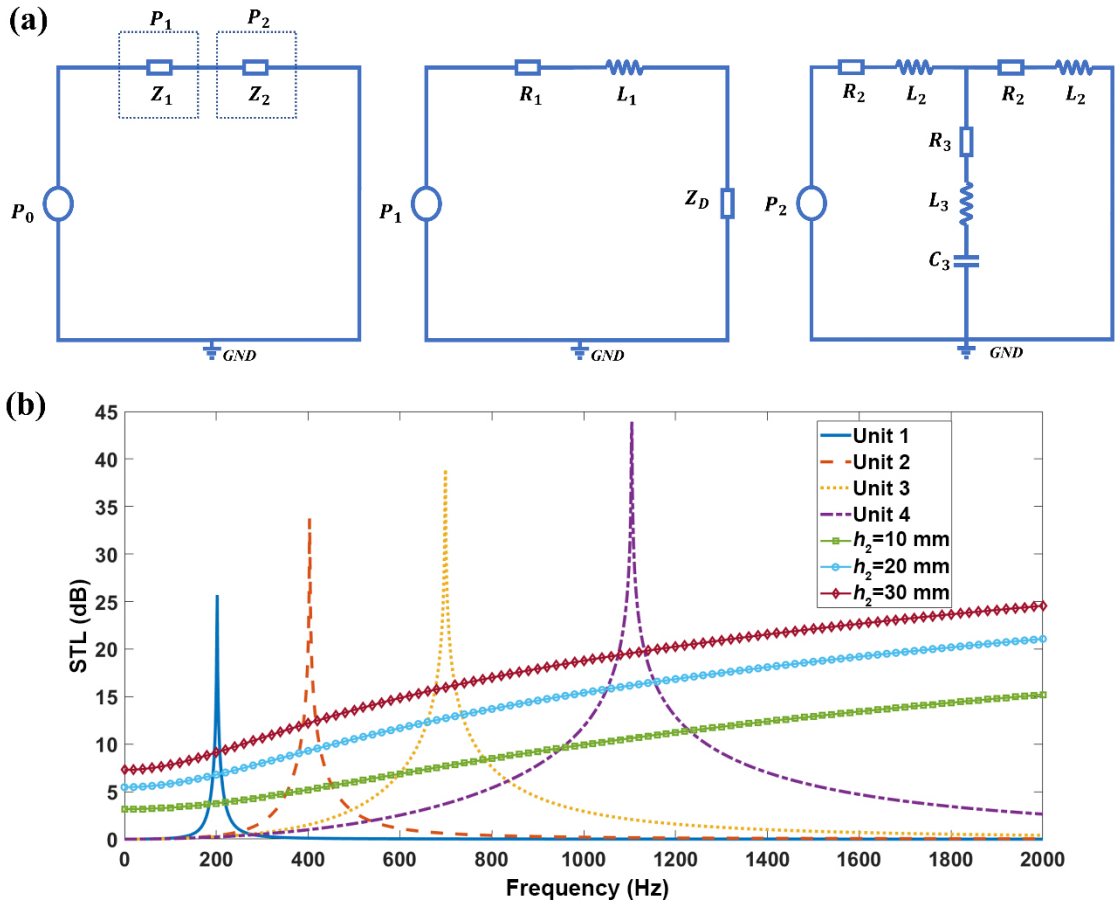


FIG. 2. (a) Acoustic-electrical analogy of acoustic metasurface muffler. The left figure is for acoustic metasurface muffler. The middle one is for micro-perforated plate. The right one is for composite waveguide. (b) The relation of transmission loss and the frequency for the micro-perforated plate with different mid-air layer thickness (rhombus, circle, and square correspond to $h_2$=10 mm, 20 mm, and 30 mm, respectively.) and different composite waveguides of units 1-4, corresponding to blue, orange, yellow, purple lines, respectively.

To further explore the underlying working mechanism, as shown in Fig. 2(a), we established the acoustic-electric analogy model of the coupled anechoic structure and obtained the changing relationship of the sound transmission loss of each part of the structure with frequency according to the acoustic local analysis method. In Fig. 2(b), here we focus on the following four frequency points of 202 Hz, 403 Hz, 698 Hz, and 1104 Hz corresponding to units 1-4, at which the capability of the coupled muffler is dominated by sound absorption induced by the visco-thermal loss and also reflection by the effective impedance mismatching. This is due to the resonance of the composite waveguide. As the frequency of the noise increases, the effect of micro-perforated plates becomes even more dramatic. According to our design, when the frequency exceeds 1100 Hz, the micro-perforated plate plays a major role in sound absorption and insulation in the coupling structure.

In brief, the AMM can realize the broadband noise elimination because of the existence of the resonance peak for the composite waveguide and the assist of the micro-perforated plate. Through the above analysis, it is proved that broadband acoustic suppression comes from the coaction of the four coupled resonant chambers. Empowered by the coupling effect, our muffler has a wide noise attenuation bandwidth. Compared with the noise cancellation structure designed solely by interference [27] or dissipation [28] mechanism, our advantage lies in making full use of the synergistic effect of resonance and dissipation to achieve low frequency and broadband noise cancellation.

### C. Numerical simulation and experimental demonstration

The designed coupled silencing structure is numerically simulated by using the "Pressure Acoustics, Frequency Domain" module of COMSOL Multiphysics, in which the frequency domain study is performed to calculate the sound transmission through the coupled silencing structure. To be consistent with experimental conditions and estimate its low-frequency behavior under plane wave incidence, the designed coupled silencing structure is emplaced in a cylindrical waveguide, both the waveguide wall and coupled silencing structure are considered acoustically rigid in the physical field settings. To avoid the effects of reflected waves, both ends of the waveguide are set as plane-wave radiation boundaries while the incident wave is plane wave and acoustic pressure amplitude is set as 1 Pa. Because there are tiny structures inside, we choose these regions as "Narrow Region Acoustics" in COMSOL, which can simulate the acoustic structures considering visco-thermal loss.

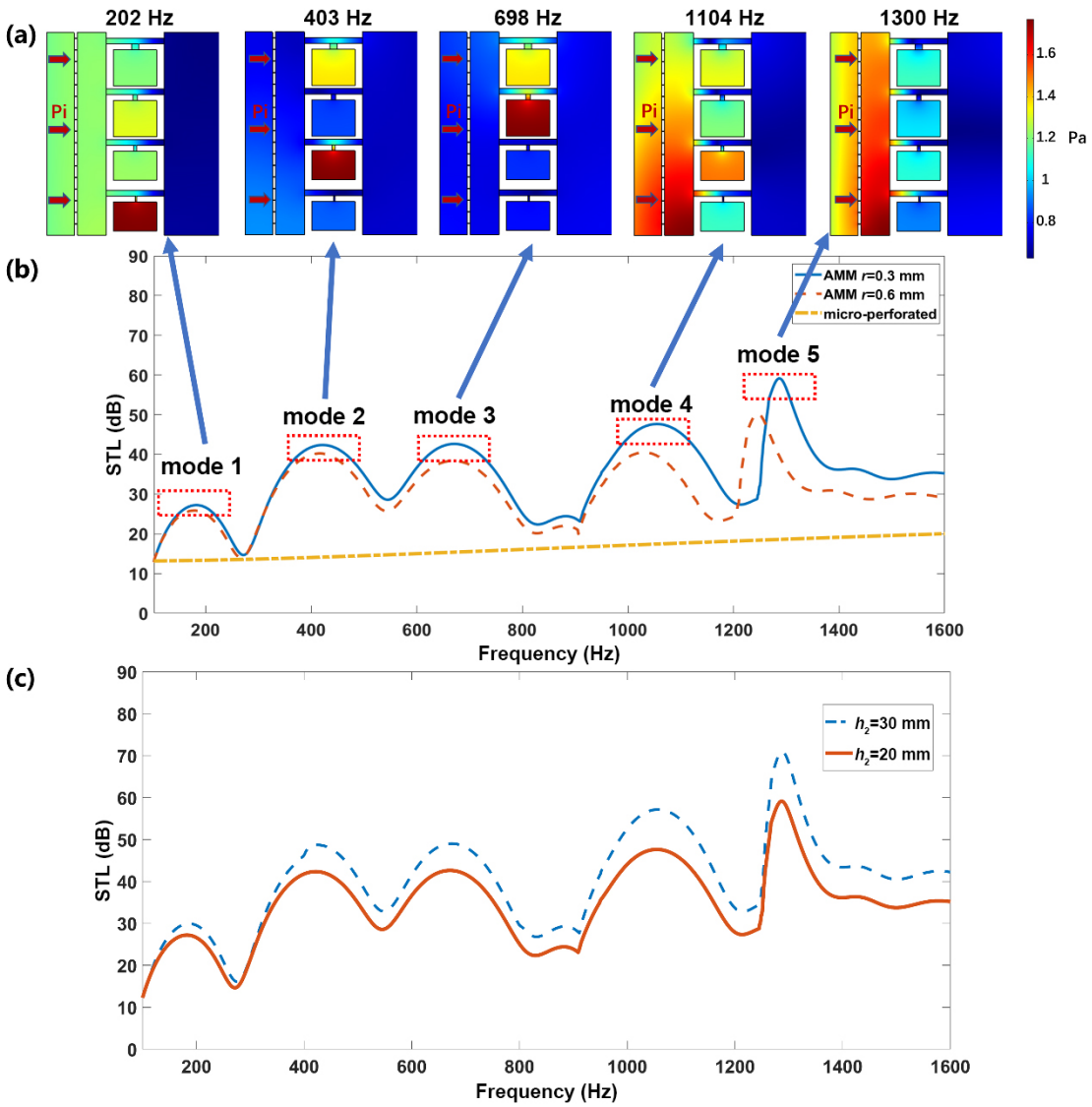


FIG. 3. (a) Sound field distribution in the structure at the frequencies of 202 Hz, 403 Hz, 698 Hz, 1104 Hz, and 1300 Hz, respectively, denoted as modes 1-5. Incident directions are marked by arrows and incident pressure is marked by Pi in the figure. (b) Simulation diagram of the STL curve of the AMM ($r$=0.3 mm and $r$=0.6 mm) and micro-perforated ($r$=0.3 mm). Modes 1-5 are marked in the figure. (c) The simulations considering the mid-air layer with different thicknesses of $h_2$=20 mm and $h_2$=30 mm, respectively.

Figure 3(a) shows the acoustic pressure amplitude distributions for different modes (modes 1-5). Incident directions are marked by arrows and the incident pressure is marked by Pi in the figure. According to the previous analysis, modes 1-3 (202 Hz, 403 Hz, 698 Hz) are mainly caused by coupling resonance of different composite waveguides, respectively, and the additional cavities formed by micro-perforated and composite waveguides. In addition, it can be seen from Fig. 3(a) that the composite waveguide structures play a major role in different vibration modes, which is related to our parameter design. For mode 4 (1104 Hz) in Fig. 3, we

find that the acoustic pressure amplitude is large not only in the third composite waveguide but also in the mid-air layer. It means the cavity of the mid-air layer between the micro-perforated plate and the composite waveguide is also resonant at 1104 Hz. Mode 4 is caused by the coupling resonant of the mid-air layer and the composite waveguide. For mode 5 (1300 Hz) in Fig. 3, we find that the composite waveguide is no longer resonant. The resonance only occurs in the mid-air layer. This is consistent with the theoretical results of the acoustic-electric analogy analysis. Figure 3(b) shows that improper selection of the parameters will reduce the STL of the structure, and the selection of the aperture of the micro-perforated plate has a great influence on the middle and high frequencies (mode 4 and mode 5). A comparison for parameters $r$=0.3 mm and $r$=0.6 mm show that $r$=0.3 mm has higher efficiency, that we choose this optimized radius as the final design. We also plot the curve for the structure with only micro-perforated plate in Fig. 3(b) as a reference. The comparison shows that the designed AMM has higher STL efficiency than micro-perforated plate. Figure 3(c) shows the simulation considering the mid-air layer with different thicknesses with $h_2$=30 mm and $h_2$=20 mm, respectively. Combining the results in Fig. 3(c) and Fig. 2(b), we find that the STL is increasing with the mid-air layer thickness. Considering the tradeoff of sample thickness and the sound insulation, we choose $h_2$=20 mm in the sample fabrication.

Meanwhile, the standard impedance tube system was used for the experimental measurement, and the double load method [20] was used for the measurement, where the sample is fixed firmly with clamps in the impedance tube. The experimental setup, consistent with that adopted in numerical modeling, is schematically illustrated in Fig. 4(a). The sample of AMM made of photosensitive resin via 3D printing is shown by the inset in Fig. 4(b). The relevant results are shown in Fig. 4(c). The parameters of the structure are consistent with those used in theoretical calculation.

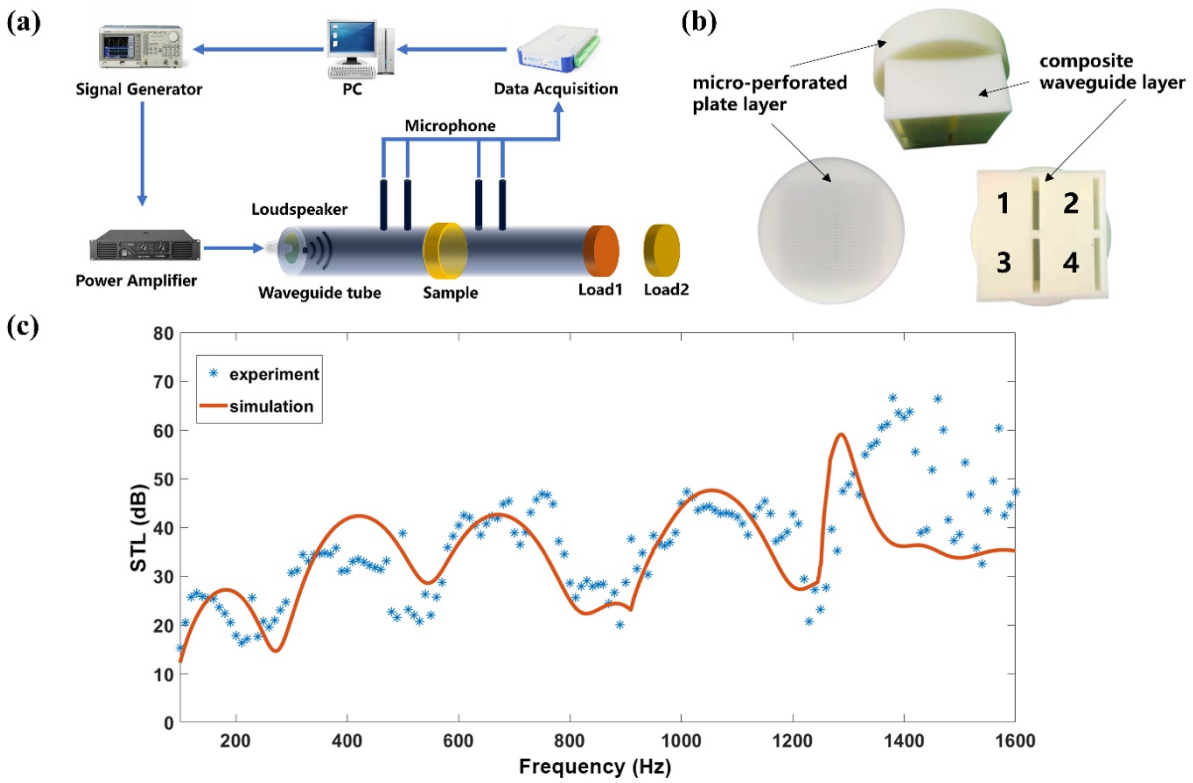


FIG. 4. Diagram of simulation and experiment results. (a) Schematics of the experimental setup for the double load method where the specimen is clamped in the impedance tube. (b) The 3D printed sample structure schematic diagram made according to the theoretical model shown in Fig. 1. Numbers 1, 2, 3, and 4 represent different composite waveguide units respectively, which correspond to Fig. 1 (Here the coupling structure is designed as prescribed by the standard impedance tube for experiments. While following the presented design strategy, it can be straightforwardly reshaped as a cube). (c) Simulated (red line), and measured (blue asterisk) sound transmission loss (STL) of the designed structure.

As can be seen from Fig. 4(c), the theoretical prediction shows excellent agreement with numerical and experimental results, demonstrating the effectiveness of our design. The designed AMM sample blocks more than 90% of incident sound energy in the range of 100−1600 Hz (experimental data). In Fig. 4(c), caused by the resonance of the composite waveguide, there are multiple peaks within 100-1600 Hz. Meanwhile, the dissipation effect of the micro-perforated plate makes the coupling muffler structure keep a high muffler capacity. More specifically, harnessing the power of dissipation in combination with resonance remarkably lowers the onset frequency in the current design. It is noted that the ‘sampled’ frequencies do not exactly coincide with the peaks. This is because modes 1-5 are inevitably affected by the coupling resonances between composite waveguides and mid-air layer. However, we consider that this effect is not obvious in the case of very low sound frequency (modes 1-3), because the resonance frequency for the mid-air layer is between modes 4-5.

For the optimization of the frequency band, the design of the fine-distributed composite

waveguide is critical in the proposed AMM. In the current study, we theoretically choose 200 Hz, 400 Hz, 700 Hz, and 1100 Hz as four targeted resonant frequencies as shown in Fig. 3(b). From mode 5 in Fig. 3, the resonant frequency for the mid-air layer is 1300 Hz. These five frequencies lead to the final broadband absorption spectrum from 100 Hz to 1600 Hz. Different unit cells are deliberately designed to have a continuous bandwidth. The resonant frequency of the composite waveguide is mainly decided by the parameters of Table 1.

## III. Conclusion

We have theoretically and experimentally introduced an analytical model to design an acoustic metamuffler. The acoustic-electrical analogy method has been applied to the theoretical analysis, and the FEM results have shown a good agreement with the experimental measurements. We have investigated an alternative metastructure composed of a composite waveguide and a micro-perforated plate. To illustrate the proposed concept and underlying physical mechanism, we have combined theory and experiment to achieve a broadband ventilated metamuffler operating at the low frequency of 100-1600 Hz, featuring a deep-subwavelength thickness. We have shown that the designed metastructure helps to enlarge the bandwidth and strengthen the effectiveness of the sound insulation at a low frequency regime.

## Acknowledgments

The authors acknowledge the financial support provided by the National Natural Science Foundation of China (No. 11874110).

## Reference

[1] X. Yu, S-K. Lau, L. Cheng, and F. Cui, A numerical investigation on the sound insulation of ventilation windows, Appl. Acoust. 117, 113 (2017).

[2] S. A. Cummer, J. Christensen, and A. Alù, Controlling sound with acoustic metamaterials, Nat. Rev. Mater. 1(3), 1-13 (2016).

[3] G. Ma, and P. Sheng, Acoustic metamaterials: From local resonances to broad horizons, Sci. Adv. 2(2), e1501595 (2016).

[4] B. Assouar, B. Liang, Y. Wu, Y. Li, and Y. Jing, Acoustic metasurfaces, Nat. Rev. Mater. 3(12), 460-472 (2018).

[5] Y. Li, B. Liang, Z. M. Gu, X. Y. Zou, and J. C. Cheng, Reflected wavefront manipulation based on ultrathin planar acoustic metasurfaces, Sci. Rep. 3, 2546 (2013).

[6] J. J. Zhao, B. W. Li, Z. N. Chen, and C. W. Qiu, Manipulating acoustic wavefront by inhomogeneous impedance and steerable extraordinary reflection, Sci. Rep. 3, 2537 (2013).

[7] J. J. Zhao, B. W. Li, Z. N. Chen, and C. W. Qiu, Redirection of sound waves using acoustic metasurface, Appl. Phys. Lett. 103(15), 151604 (2013).

[8] Y. Li, and B. Assouar, Acoustic metasurface-based perfect absorber with deep subwavelength thickness, Appl. Phys. Lett. 108(6), 204301 (2016).

[9] S. Huang, X. Fang, X. Wang, B. Assouar, Q. Cheng, and Y. Li, Acoustic perfect absorbers via spiral metasurfaces with embedded apertures, Appl. Phys. Lett. 113(23), 233501 (2018).

[10] K. Donda, Y. Zhu, S. W. Fan, and B. Assouar, Extreme low-frequency ultrathin acoustic absorbing metasurface, Appl. Phys. Lett. 115(17), 173506 (2019).

[11] X. Wu, K. Y. Au-Yeung, X. Li, R. C. Roberts, J. Tian, C. Hu, Y. Huang, S. Wang, Z. Yang, and W. Wen, High-efficiency ventilated metamaterial absorber at low frequency, Appl. Phys. Lett. 112, 103505 (2018).

[12] L. J. Li, B. Zheng, L. M. Zhong, J. Yang, B. Liang, and J. C. Cheng, Broadband compact acoustic absorber with high-efficiency ventilation performance, Appl. Phys. Lett. 113, 103501 (2018).

[13] R. Ghaffarivardavagh, J. Mikolajczyk, S. Anderson, and X. Zhang, Ultra-open acoustic metamaterial silencer based on fano-like interference, Phys. Rev. B. 99, 024302 (2019).

[14] S. Huang, Z. Zhou, D. Li, T. Liu, X. Wang, J. Zhu, and Y. Li, Compact broadband acoustic sink with coherently coupled weak resonances, Sci. Bull. 65, 373-379 (2020).

[15] Y. F. Zhu, K. Donda, S. W. Fan, L. Y. Cao, and B. Assouar, Broadband ultra-thin acoustic metasurface absorber with coiled structure, Appl. Phys. Express 12(11), 114002 (2019).

[16] Y. F. Zhu, and B. Assouar, Nonlocal acoustic metasurface for ultra-broadband sound absorption, Phys. Rev. B, 103(6), 064102 (2021).

[17] R. Z. Dong, Mao. D, X. Wang, X. W, and Y. Li, Ultra-broadband acoustic ventilation barriers via hybrid-functional metasurfaces, Phys. Rev. Appl. 15, 024044 (2021).

[18] H. L. Zhang, Y. F. Zhu, B. Liang, J. Yang, J. Yang, J. C. Cheng, Omnidirectional ventilated acoustic barrier, Appl. Phys. Lett. 111(20), 203502 (2017).

[19] T. Lee, T. Nomura, E. M. Dede, and H. Iizuka, Ultrasparse acoustic absorbers enabling fluid flow and visible-light controls, Phys. Rev. Appl. 11, 024022 (2019).

[20] M. Sun, X. S. Fang, D. X. Mao, X. Wang, and Y. Li, Broadband acoustic ventilation barriers, Phys. Rev. Appl. 13, 044028 (2020).

[21] H. Zhang, Z. Wei, X. Zhang, L. Fan, J. M. Qu, and S. Y. Zhang, Tunable acoustic filters assisted by coupling vibrations of a flexible Helmholtz resonator and a waveguide, Appl. Phys. Lett., 110(17), 1315-829 (2017).

[22] D. Y. Maa. Potential of microperforated panel absorber, J. Acoust. Soc. Am. 104, 2861–6 (1998).

[23] X. Yu, L. Cheng, and X. You, Hybrid silencers with micro-perforated panels and internal partitions, J. Acoust. Soc. Am. 137, 951–62 (2015).

[24] J. Kang, and M. W. Brocklesby, Feasibility of applying micro-perforated absorbers in acoustic window systems, J. Appl. Acoust. 66, 669–89 (2005).

[25] M. Yang, S. Y. Chen, C. X. Fu, and P. Sheng, Optimal sound-absorbing structures. Mater. Horiz. 4(4), 673-680 (2017).

[26] L. Kinsler, Fundamentals of Acoustics (Wiley, New York, 1982).

[27] J. Yang, J. S. Lee, H. R. Lee, Y. J. Kang, and Y. Y. Kim, Slow-wave metamaterial open panels for efficient reduction of low-frequency sound transmission, Appl. Phys. Lett. 112, 091901 (2018).

[28] S. Kumar, and H. P. Lee, Labyrinthine acoustic metastructures enabling broadband sound absorption and ventilation, Appl. Phys. Lett. 116, 134103 (2020).